Macromolecules

Article

Cite This: Macromolecules 2018, 51, 2283−2292

Selective Swelling of Electrospun Block Copolymers: From Perforated Nanofibers to High Flux and Responsive Ultrafiltration Membranes

Xiansong Shi,[†] Zhi Xu,[‡] Chaobo Huang,[§] Yong Wang,*[,†] and Zhanfeng Cui[‡]

[†]State Key Laboratory of Materials-Oriented Chemical Engineering, College of Chemical Engineering, and Jiangsu National Synergetic Innovation Center for Advanced Materials, Nanjing Tech University, Nanjing 210009, P. R. China

[‡]CRMI Technology Centre, Institute of Biomedical Engineering, Department of Engineering Science, University of Oxford, Oxford, U.K.

[§]College of Chemical Engineering, Jiangsu Key Lab of Biomass-based Green Fuels and Chemicals, Nanjing Forestry University, Nanjing 210037, P. R. China

Supporting Information

ABSTRACT: This work is devoted to the development of high-flux ultrafiltration membranes using electrospun nanofibers of amphiphilic block copolymers (BCPs) of polystyrene-*block*-poly(2-vinylpyridine) (PS-*b*-P2VP) as building blocks. When soaked in hot ethanol, the solid as-spun BCP fibers are progressively transformed into three-dimensionally perforated fibers with increasing porosities with rising degrees of swelling, which ended up with the equilibrated morphology of spherical micelles. The BCP nanofibers are collected on macroporous substrates and subjected to heating to convert loosely stacked fibers to dense and continuous films. Subsequent swelling in hot ethanol leads to robust composite membranes with nanoporous BCP selective layers tightly adhered to the substrates. Filtration performances of the composite membranes can be conveniently modulated by electrospinning durations. The water permeabilities are as high as 6100 L m^{-2} h^{-1} bar^{-1}, which is ∼10−35 times higher than that of commercial membranes with similar rejections. Moreover, with the surface enrichment of P2VP chains the membranes exhibit a strikingly sharp pH-dependent water permeability switchable in the largest amplitude ever reported for multiple cycles. Electrospun fibers can be promising building materials to produce a wide range of membranes with 3D interconnected nanoporosities which also show great potential in separation and biomedical applications.

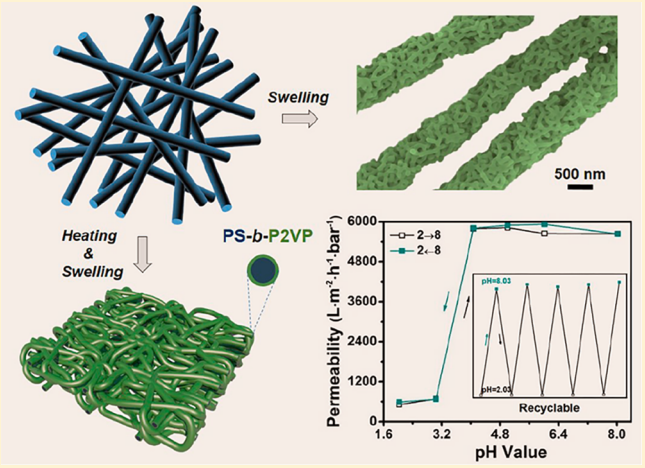

Electrospun fibers have been demonstrated to be promising building blocks to provide a simpler and more cost-effective means to produce structures with an interconnected pore and fiber diameters in a nanometer scale. The versatility of the technique has allowed for spinning of a very diverse set of matrix, such as scaffold for tissue engineering and membrane for separation.[1−5] The scaffold produced by the electrospinning process has a high surface area-to-volume ratio, providing more substrate for cell attachment and a higher cell density per unit of space compared to other structures.[6] While the membranes built from electrospun fibers are usually featured with micrometer-sized pores, they can be directly applied in microfiltration (MF) processes to efficiently remove micrometer- or submicrometer-sized particles from water.[7−9] Ultrafiltration (UF) membranes with pore sizes in the range of ∼1−100 nm exhibit a much tighter selectivity than MF membranes, and they can effectively remove colloids, virus, proteins, and endotoxin to provide potable water.[10,11] Therefore, to repel smaller particles from water, the effective pore sizes of nanofibrous membranes should be reduced down to the UF category. To this end, Hsiao and co-workers developed a number of methods to build dense but water-permeable barrier layers on the surfaces of electrospun nanofibrous substrates to obtain UF selectivities.[12−14] For instance, they coated hydrogel layers on electrospun nanofibrous membranes and produced UF membranes which were able to remove oil-in-water nanoemulsions from water.[12] Additionally, they electrospun nanofibers of copolymers containing both hydrophobic and hydrophilic segments on macroporous substrates and exposed them to solvents to swell the hydrophilic polymers followed by cross-linking, sealing the gaps between the original nanofibers

Received: January 30, 2018
Published: March 12, 2018

DOI: 10.1021/acs.macromol.8b00220
Macromolecules 2018, 51, 2283−2292

with cross-linked hydrogel films. Thus-produced membranes exhibited excellent retentions to proteins while allowed water to penetrate through the cross-linked hydrogel.[15] However, the barrier layers of hydrogel posed a significant flow resistance to water and membranes with such barriers as the selective layers suffered from low permeabilities. Alternatively, Menkhaus et al. demonstrated another strategy for preparing UF membranes by grafting polymer chains to the surface of electrospun nanofibrous membranes, and the produced membranes were demonstrated to effectively remove 40 nm nanoparticles from water.[16] Unfortunately, the grafting polymer chains inevitably reduced the effective pore sizes of nanofibrous membranes, which in return led to a significant decline in water permeabilities. Water permeabilities of UF membranes derived from electrospun fibers are typically lower than 100 L m^{-2} h^{-1} bar^{-1}, which are generally lower than that of UF membranes prepared by the traditional process of nonsolvent-induced phase separation.[17] That is, the high-flux advantage of the electrospun nanofibrous substrates does not play an effective role in reducing the flow resistance of the targeted UF membranes. Therefore, it remains challenging to produce high-flux UF membranes using electrospun nanofibers as building blocks.

Previous studies reveal that UF membranes can be achieved by reducing the size of the gaps between neighboring fibers either by expanding the diameters of the nanofibers induced by swelling or by incorporating additional materials to the fiber surface. However, the porosities will be sacrificed with the reduction of the pore size, resulting in significantly reduced water permeabilities. This trade-off effect can be overcome if one can create accessible nanopores throughout the expanding nanofibers, thus providing additional channels for water permeation. The pores should be perforated through the fibers to allow water to access, and their size should not exceed the UF category to ensure a desired selectivity.

There are a number of methods reporting the fabrication of porous electrospun nanofibers. It has been reported that electrospinning in high humidity can produce nanofibers with nanopores on the fiber surface.[18] However, these pores were formed as a consequence of templating effect of condensed water droplets, and they only appeared on the fiber surface as shallow concaves and did not present an interconnected porosity. Alternatively, nanoporous fibers can be prepared by electrospinning block copolymers (BCPs) containing labile blocks followed by selectively etching away the microdomains composed of the labile blocks.[19] However, the resultant porous fibers frequently suffer from an inadequately developed porosity due to the incomplete removal of sacrificial components, leading to impermeable "dead-end" pores. Moreover, the need for the selective etching of one component makes pore generation process much more complicated and requires harsh etching conditions. Recently, we developed a versatile method to generate nanopores in BCP materials, which has been termed as selective-swelling-induced pore generation.[20] The selective swelling cavitation approach is capable of creating nanopores in BCPs with any dimension including one-dimensional (1D) nanorods, 2D ultrathin films, and 3D bulk materials.[21−23] In selective swelling, there is a considerable volume expansion up to ∼200% of the BCP materials.[24] Moreover, our previous works on selective swelling cavitation of BCP nanorods revealed that 3D interconnected nanoporosities could be obtained,[21,25] implying the feasibility to fabricate highly permeable UF membranes by using BCP electrospun fibers as the building blocks on which selective swelling is performed to cavitate the fibers.

In this work, an amphiphilic BCP, polystyrene-*block*-poly(2-vinylpyridine) (PS-*b*-P2VP), was electrospun to prepare continuous nanofibers. We first investigated the swelling behaviors of the as-spun nanofibers in hot ethanol, confirming the cavitation accompanied by increasing porosities and diameter of the fibers with increasing degree of swelling. The electrospun BCP fiber layers were then composited with macroporous substrates and heated to enhance the adhesion of fibers to other fibers and to the substrate. Subsequently, the fiber layer on top of the substrate was soaked in hot ethanol to expand and also to cavitate the fibers by the mechanism of selective swelling (Figure 1). The original fibrous structure with

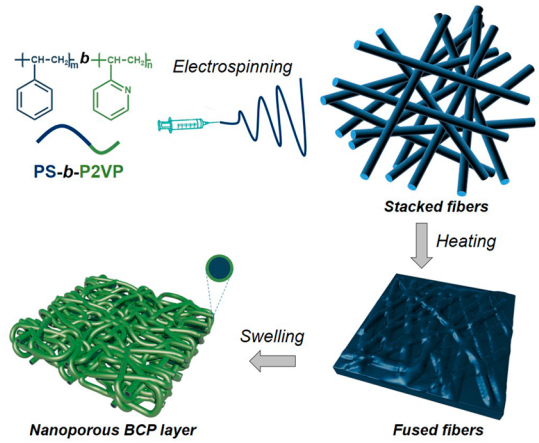

Figure 1. Schematic representation of the preparation process for the UF membranes from BCP electrospun nanofibers.

micrometer-sized pores was converted to a nanoporous layer containing 3D-interconnected pores with sizes of several tens of nanometers, thus producing a composite membrane with the nanoporous BCP layer delivering a UF selectivity. Thus-produced UF membranes exhibit exceptionally high water permeabilities, which are approximately 10−35 times higher than commercial UF membranes with a similar rejection. Moreover, with the enrichment of P2VP on the pore wall, the membranes also display very sensitive pH-dependent water permeability switchable in the largest amplitude ever reported. The strategy of fabricating 3D interconnected network by combining electrospinning BCPs and selective swelling could further extend to scaffold constructions in tissue engineering and meets their requirements on high specific surface area and porosity.

RESULTS AND DISCUSSION

Selective Swelling of Electrospun BCP Nanofibers. Under fixed electrospinning conditions as stated in Materials and Methods section, we were able to produce continuous BCP nanofibers with relatively uniform diameters. It should be noted that a small amount of lithium chloride (LiCl, 0.03 wt % to the spinning solution) was incorporated into the spinning dopes to enhance their conductivity,[26] preventing the formation of beaded structures (Figure S1). We first used silicon wafers as the substrates to collect the electrospun fibers. As can be seen from Figure S1b, silicon wafers were partly covered by overlapped BCP nanofibers after electrospinning for approximately 1 min. The BCP nanofibers exhibited a smooth surface

DOI: 10.1021/acs.macromol.8b00220
Macromolecules 2018, 51, 2283−2292

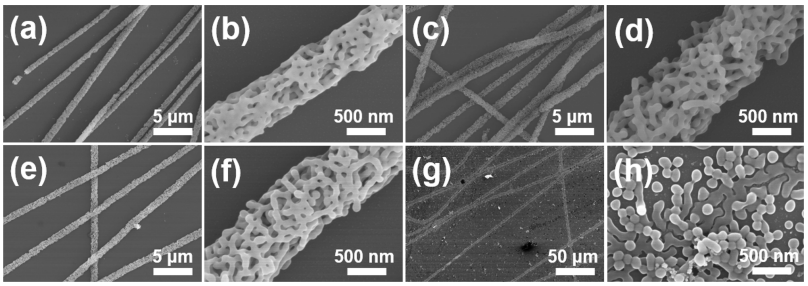

Figure 2. SEM images of BCP electrospun nanofibers after swelling in ethanol under various conditions: 70 °C for 1 h (a, b) and 6 h (c, d), and 75 °C for 1 h (e, f) and 6 h (g, h).

and a relatively uniform diameter of ~620 ± 42 nm (Figure S1c). To obtain perforated BCP nanofibers, we immersed the electrospun nanofibers in hot ethanol at different temperatures for various durations. After immersion in ethanol at 70 °C for 1 h, the fiber diameter was increased to ~830 ± 153 nm (Figure 2a). A closer scanning electron microscopy (SEM) examination reveals that the nanofibers take a perforated, nanoporous morphology (Figure 2b), which is in stark contrast to the initially solid, nonporous structure before swelling (Figure S1c). With an extended swelling duration of 6 h, the fiber diameter was further increased to ~940 ± 109 nm (Figure 2c). As clearly shown in Figure 2d, these fibers exhibited a more pronounced porous structure, which can be described as networks composed of 3D interconnected struts with a uniform diameter of about 74 nm. Gaps between interconnected struts define the pores and the pore diameters are a few tens of nanometers.

The perforation of the BCP nanofibers is enabled by the mechanism of selective swelling-induced pore generation.[20,27,28] We previously demonstrated that selective swelling was able to generate nanoporosities in 1D BCP nanorods and 3D bulk materials.[21,23] The BCP electrospun nanofibers investigated here present a diameter bigger than 600 nm, much larger than the bulk period of the BCP. Consequently, their perforating behaviors by selective swelling is considered to be similar to that of BCP bulk materials. For the as-spun BCP nanofibers, the P2VP phases are randomly dispersed in the PS matrix as isolated cylinders because the volume fraction of P2VP in the BCP is 28.4%, which corresponds to a cylindrical morphology according to the phase diagram of BCPs.[29] When immersed in hot ethanol which has a much stronger affinity to P2VP than to PS, the P2VP cylinders are swollen and expanded in size with the uptake of ethanol. Thus, the originally isolated P2VP cylinders are approaching and connected with each other, forming a continuous phase distributed throughout the PS matrix. The swelling P2VP phases force the PS matrix to expand to some extent. The expansion of the PS matrix is enabled by the plastic deformation as a result of enhanced segmental mobility of PS chains in hot ethanol. However, it should be noted that the PS phases are still in the glassy state, and therefore the fibers largely maintain their initial shapes. Upon drying, with the loss of ethanol the P2VP chains are collapsed whereas the PS chains cannot recover to their initial position in the absence of driving force. Therefore, empty interspaces are generated in the positions of the initially swollen P2VP phases; that is, the PS skeleton is wrapped by collapsed P2VP chains, forming an interconnected perforated nanoporous structure. After immersion in ethanol for longer durations or at higher temperatures, the P2VP cylinders are swollen to higher degrees, correspondingly leading to more pronounced porous morphologies.

Swelling temperatures play an essential role in controlling the swelling kinetics and the morphology of the nanofibers. Generally, elevated swelling temperatures enhance the perforation process. As shown in Figure 2e,f, swelling at 75 °C for 1 h leads to porous nanofibers with a diameter of ~920 ± 83 nm, which is much larger than that of nanofibers produced by swelling at 70 °C for the same duration (1 h). However, prolonged swelling at 75 °C for 6 h breaks up the original fibrous morphology. As shown in Figure 2g,h, the 3D networks of interconnected struts observed before are decomposed, leaving behind of flattened networks adhering on the substrate surface and also nanospheres scattering around the flattened networks. The diameters of the nanospheres and the struts consisting of the network are both around 130 nm. We note that the arrangement of the flatted networks and the nanospheres on the substrate is still reminiscent of the position and the orientation of the original nanofibers although they are distributed in much wide zones than the diameter of the original fibers. Moreover, there are also nanospheres dispersed in ethanol used to swell the nanofibers, which can be collected by membrane filtration. These nanospheres are spherical micelles with PS cores and P2VP coronae. These micelles are formed through the mechanism of heating-enabled micellization.[30] At elevated temperature, the affinity between ethanol and the polymer chains as well as the segmental mobility of both PS and P2VP blocks is enhanced, triggering the micellization of PS-*b*-P2VP in ethanol. The composition of the micelles with PS cores and P2VP coronae has been clearly confirmed by transmission electron microscopy.[30] Such a morphological transition from the original solid state to increasingly pronounced perforated states ending up with spherical micelles has also been observed in our previous works of selective swelling of BCP films and nanorods.[20]

The increase in diameters of the fibers is merely caused by the introduction of pores into the fibers, and therefore we can estimate the porosities of the perforated fibers by comparing the diameter of the nanofibers before and after swelling if we assume that the volume expansion of the fibers only occurs in the radical direction and the fibers maintain a regular cylindrical morphology. More specifically, the porosities of the nanofibers after swelling were calculated by the following equation:

$$\%P = 100 \times (D_s^2 - D_p^2)/D_s^2 \quad (1)$$

where D_p and D_s are the fiber diameters before and after ethanol swelling. We estimate that swelling the nanofibers in ethanol at 70 °C for 1 and 6 h produce a porosity of 44.2% and 56.5%, respectively, indicating the highly porous state of the swelling-treated nanofibers. The porosity of the nanofibers subjected to ethanol swelling at 75 °C for 1 h is estimated to be

DOI: 10.1021/acs.macromol.8b00220
Macromolecules 2018, 51, 2283−2292

54.6%, confirming the more pronounced perforation at higher swelling temperatures. We purposely cut the fibers to expose their interior structures. As clearly shown in Figure 3, the

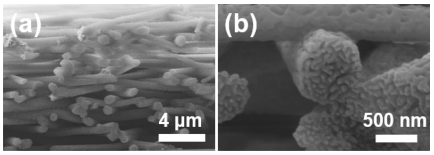

Figure 3. SEM images at different magnifications showing the morphology of the perforated BCP fibers (subjected to ethanol swelling at 70 °C for 1 h) cut to expose the interior structure.

exposed ends of the ethanol-treated fibers show an interconnected porous morphology similar to that on their surface, indicating that through such a swelling treatment in ethanol the fibers are completely perforated and the pores are 3D interconnected, forming a continuous phase interlaced in the fibers. Such open porous structures promise high surface areas and are easily accessible to foreign substances and therefore are expected to have significantly enhanced mass transfer which is important in many applications include bioengineering,[31] catalysis,[32] separation,[33] etc.[34,35]

Fabrication of UF Membranes Using BCP Electrospun Nanofibers as Building Blocks. After demonstration of the perforation of BCP electrospun nanofibers by selective swelling, we then investigated the feasibility of producing selective membranes using the BCP electrospun nanofibers as building blocks. We first directly treated the electrospun BCP nanofibers in hot ethanol. Although ethanol swelling produces nanopores in each fiber, however, the pores defined by the gaps between neighboring fibers in the stacked fibers are still in the range of a few micrometers (Figure S2), which determine the permselectivity of the fiber layers in membrane separation, and the fiber layers still can only behave as MF membranes. Even worse, the fiber layers do not possess a strong adhesion to the porous substrate, and they tend to shrink and are easily peeled off from the substrate. Alternatively, we adopted a heating treatment to the fiber layers before selective swelling. The heating treatment was carried out at the temperature of 110 °C, which is slightly higher than the glass transition temperature (T_g) of both PS and P2VP.[36] Consequently, the densely stacked nanofibers were partially melt[37] and merged as a continuous layer, forming continuous layers tightly adhered to the macroporous poly(vinylidene fluoride) (PVDF) substrates. The choice of the heating temperature is critical because it should be high enough to melt individual fibers to form a continuous layer and to enhance the adhesion of the fibers to the substrate, on one hand, and it should not be much higher than T_g of blocks to prevent leaking of the completely melt BCPs into the porous substrate, on the other. We also tried heating the sample at 100 °C, which was very close to T_g of both blocks; however, the BCP layer easily detached from the PVDF substrate in the subsequent swelling treatment because of the poor adhesion between the two layers.

The morphological changes that occurred after heating treatment of the BCP fiber layers were examined by SEM. In the as-spun fiber layers, the fibers are randomly stacked with each other and pores sizes from hundreds of nanometers to a few micrometers are formed by overlapped fibers (Figure 4a). After heating at 110 °C for 1 h, the originally stacked structure of BCP fibers collapses, and the fibers are fused with their

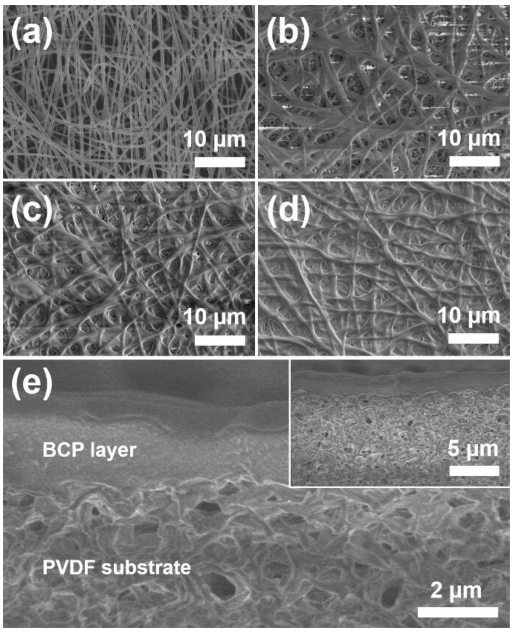

Figure 4. SEM images of BCP fiber layers before and after heating at 110 °C for 1 h: (a) surface morphology of the as-spun BCP fiber layers before heating; (b–d) surface morphology of the heated BCP fiber layers with an electrospinning duration of 0.5 h (b), 1 h (c), and 2 h (d); (e) Cross-sectional morphology of the heated BCP fiber layers with 1 h electrospinning; inset shows a large-field view of the cross section.

neighbors to generate a relatively dense layer on top of the PVDF substrate. However, the heated BCP layers still show a fibrous morphology (Figure 4b–d). More specifically, with the electrospinning duration as short as 0.5 h, because of the thin thickness of the fiber layer pores with sizes of a few micrometers remain on the heated BCP layer and the underneath PVDF substrate can be observed through these remaining pores. With the electrospinning duration prolonged to 1 h, the remaining pore sizes in the heated fiber layers are decreased to a few hundreds of nanometers (Figure 4c), and the heated fiber layer with an electrospinning duration of 2 h seems to completely cover the PVDF substrate (Figure 4d). Figure 4e displays the cross-sectional morphology of the heated BCP layer with an electrospinning duration of 1 h, revealing a bilayered composite structure with a thin and dense top layer sitting on the underneath PVDF substrate. In contrast to the cross-sectional morphology of the as-spun fiber layer before heating, no fibrous morphology can be observed in the heated fiber layers.

We then performed selective swelling to the heated fiber layers composited on PVDF substrates to create pores in the BCP layers. The selective swelling was carried out in ethanol at 70 °C for 6 h for all the samples. Figures 5a and 5b give large-field views of the sample with 0.5 h electrospinning after selective swelling. The morphological feature is significantly different from the heated fibrous layer before selective swelling. The original fibrous morphology disappeared whereas a uniform and defect-free covering layer with a relatively smooth surface is formed. This can be ascribed to the volume expansion of the BCP fibers during swelling, which further forces the originally isolated fibers to be connected and glued with each other. The enlarged SEM image shown in Figure 5c reveals a 3D-interconnected porous morphology, which is similar to the

DOI: 10.1021/acs.macromol.8b00220
Macromolecules 2018, 51, 2283–2292

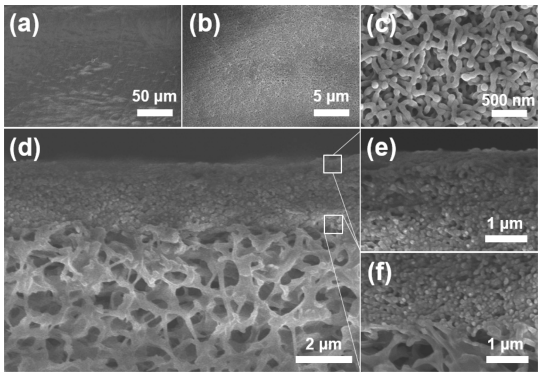

Figure 5. SEM images of the heated BCP fibrous mat prepared with an electrospinning duration of 0.5 h after ethanol swelling: (a–c) surface morphology at different magnifications; (d) cross-sectional morphology; (e, f) magnified morphological features of the corresponding boxed areas in (d).

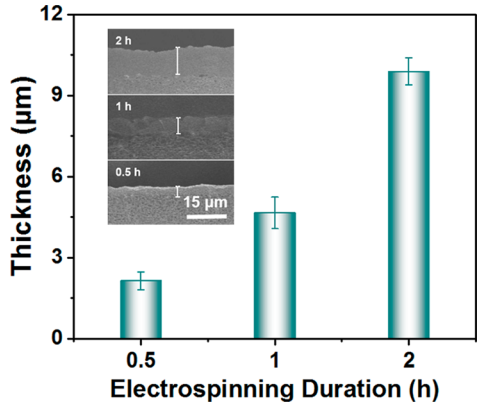

Figure 6. Dependence of the thickness of the nanoporous BCP layers on the electrospinning duration. Insets show the cross-sectional SEM images of the corresponding membranes.

porous morphology of the isolated BCP fibers after selective swelling in ethanol (Figure 2d,f). Here, we should note that samples with the electrospinning duration of 1 and 2 h possess a similar nanoporous surface (Figure S3). From the surface SEM images, we can roughly estimate that the pore sizes scatter in the range from ~30 to ~100 nm. However, because of the swelling effect of P2VP chains attached to the pore wall the effective pore sizes exhibiting in the filtration applications should be smaller depending on the environmental pHs, which will be discussed later. The pore formation in the heated BCP fibrous layers also follows the mechanism of the selective-swelling-induced pore generation as we discussed for the perforation of isolated BCP fibers. Figure 5d presents the cross-sectional morphology of the composite membrane with a 0.5 h electrospinning duration after swelling, which clearly displays a bilayered structure with a nanoporous BCP layer as the barrier and the macroporous substrate as the support. Additionally, the cross-sectional SEM images shown in Figure 5e,f evidence that the nanopores form a homogeneous network penetrating through the entire thickness of the BCP layer without a gradient in pore sizes. Moreover, the cross-sectional images reveal a seamless interface, which implies a strong adhesion between the BCP layer and the PVDF substrate.

The thickness of the nanoporous BCP layer after swelling is dependent on the amount of electrospun BCP fibers, which can be easily controlled via the duration of the electrospinning process. The thicknesses of the nanoporous BCP layers were examined by SEM imaging. As shown in Figure 6, the thickness of the BCP layer is increased from ~2.1 to ~4.6 μm and to ~9.9 μm by extending the electrospinning duration from 0.5 to 1 and 2 h, respectively, indicating the thickness is proportional to the electrospinning duration.

Surface Properties of the Membranes from BCP Electrospun Nanofibers. According to the mechanism of selective swelling, the pore generation process leads to the migration of P2VP blocks to the pore walls and to the external surface of the nanoporous BCP layers.[38] We used X-ray photoelectron spectroscopy (XPS) to analyze the surface compositions of the BCP layer at different stage of treatment. As shown in Figure 7a, the wide scan spectra displays two major emission peaks at 284 and 399 eV, which are ascribed to C 1s and N 1s, respectively. Because nitrogen atom exists only in the pyridyl groups of the P2VP blocks, the atomic ratio of nitrogen to carbon (N/C) reflects the content of P2VP chains on the surface of the BCP layer. The average N/C value of PS-*b*-P2VP used in this study can be estimated to be 3.68% based on the molecular weights of the two blocks.The N/C value of the as-spun BCP nanofiber layer is 4.37%, which is close to the average N/C value. The result implies that the PS chains and P2VP chains are randomly distributed on the surface of BCP nanofibers after spinning. Interestingly, the value is reduced to 1.50% after heating, which is much lower than the average value, suggesting that the PS chains are enriched on the outer surface of the fiber layer. The heating treatment is carried out above the T_g of both PS blocks; consequently, the polymer chains has enhanced segmental mobility. The PS chains have a lower surface energy than the P2VP chains;[39] therefore, they migrate on the fiber surface to have an energy-favorable exposure to low-surface-energy air. In contrast, the value is significantly increased to 8.79% after swelling in ethanol as a result of the higher affinity of P2VP to ethanol. Moreover, the peak of nitrogen centering around 399 eV also shows a decreased intensity after heating and then a remarkable increased intensity after swelling, which is in line with the results of N/C values (Figure 7b).

We also investigated the surface wettability of the BCP layers, and the results are shown in Figure 8. Intriguingly, the as-spun BCP fiber layer displays a strong hydrophobicity with a water contact angle (WCA) of ~130° although both PS and P2VP have the intrinsic WCAs of less than 100°.[40] This is because that the rough surface caused by the stacking fibers (Figure 4a) provides air cushions, leading to a strongly hydrophobic surface which could be theoretically described by the Cassie–Baxter model.[41] In contrast, after heating the WCA of the fiber layer is decreased to ~100°, which is still higher than that of PS homopolymers (~90°). This can be attributed to the much reduced surface roughness after heating (Figure 4b). We note that the both the as-spun and the heated BCP layers produced from various electrospinning durations give similar WCAs. After swelling treatment in ethanol, the WCA is significantly decreased to around 60°, confirming a hydrophilic surface. Additionally, because of the hydrophobic nature of the as-spun and heated BCP layers, water droplets remain sitting on these surfaces with unchanged WCAs. However, water droplets wet the surface and permeate into the interior of the swelling-treated BCP layer within a few seconds, demonstrating the easy accessibility of the pores. Moreover, we found that water droplets took short time to penetrate into the BCP layers produced with shorter electro-

DOI: 10.1021/acs.macromol.8b00220
Macromolecules 2018, 51, 2283–2292

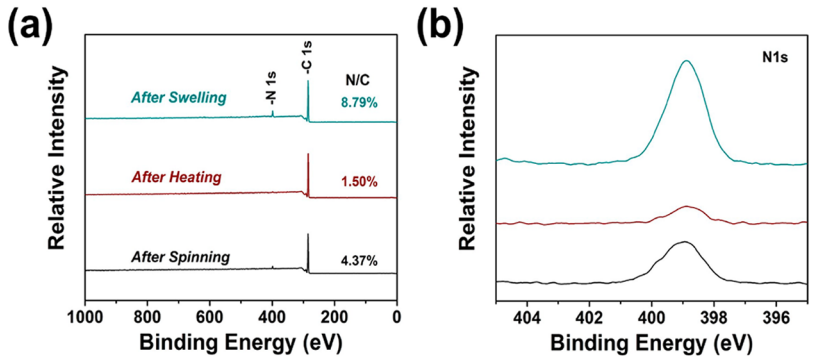

Figure 7. XPS spectra of the BCP electrospun fibers subjected to different treatments: (a) wide scan spectra; (b) high-resolution spectra detailing N 1s peaks.

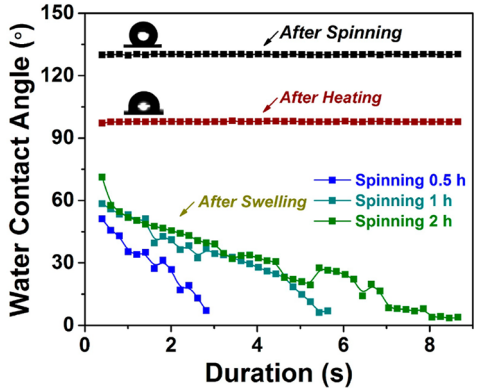

Figure 8. Water contact angles of the BCP layer after spinning, heating, and ethanol swelling.

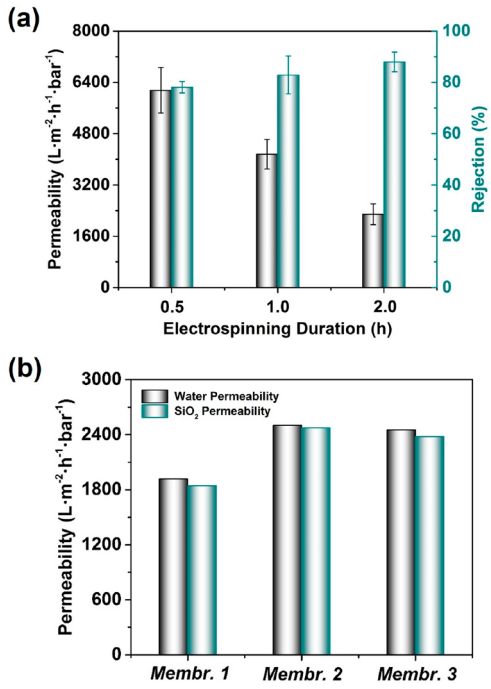

Figure 9. (a) Pure water permeabilities and rejection rates to 22 nm silica nanospheres of membranes prepared with varied electrospinning durations. (b) Comparison between permeability of the membrane with the same electrospinning duration of 2 h in the filtration of pure water and silica suspension.

spinning durations because of the lower flow resistance as a result of their thinner thickness.

Permselectivity of the Membranes from Electrospun BCP Nanofibers. The quick penetration of water into the swelling-treated BCP layers implies that the resulted bilayered structures would serve as membranes with the nanoporous BCP top layers as the selective layers. Figure 9a displays the pure water permeabilities and rejection rates to 22 nm silica nanospheres of membranes produced from BCP fiber layers with varied electrospinning durations. The bare PVDF substrate shows a water permeability of ~15 000 L m^{-2} h^{-1} bar^{-1} and a negligible retention to the silica nanospheres. After electrospinning the BCP nanofibers on the PVDF substrate followed by heating and ethanol swelling, the rejection of the membrane is significantly increased from ~0 to ~78% at the acceptable cost of a reduced permeability of ~6156 L m^{-2} h^{-1} bar^{-1}. With a spinning duration of 1 h, the permeability is decreased to ~4159 L m^{-2} h^{-1} bar^{-1} while the rejection rate is promoted to ~83%. Prolonging the spinning duration to 2 h, the resulting membrane exhibits a further decreased permeability of ~2290 L m^{-2} h^{-1} bar^{-1} and a rejection of ~88%. Such permselectivities clearly indicate that the produced membranes are in the UF category, delivering high permeabilities and a moderate selectivities. As shown in Figure 9a, there is also roughly a linear relationship between the permeabilities and the electrospinning durations, which is consistent with the observation of the linearly increased thicknesses of the nanoporous layers with prolonged spinning durations. Because the pore sizes in the BCP layers of the three membranes do not show observable differences, the increase in the thickness of the BCP layers would intensify the trans-membrane resistance,[42] leading to a continuous decline in water permeability. Furthermore, the successive promotion in rejection rates is also ascribed to the increased thickness of the nanoporous BCP layers. One may argue that the rejection to silica nanospheres may also be caused by the adsorption of the nanospheres to the BCP layers. However, we checked the membranes after filtration by SEM and observed no noticeable adsorption because conditioning in the anionic Acid Orange 7 (AO7) solution endows the membrane a negatively charged surface preventing the adsorption of negatively charged silica nanospheres (Figure S4). We also compared the concentration of silica in the feed, permeate, and retentate and found that the retentate contained higher concentration of silica than the feed (Table S1). Moreover, the permeability of the membrane with a spinning duration of 2 h in the filtration of silica suspension was compared with pure water permeability (Figure 9b). The

DOI: 10.1021/acs.macromol.8b00220
Macromolecules 2018, 51, 2283−2292

permeability in the filtration of silica suspension shows a negligible decline (<4%) compared to pure water permeability. These observations also confirm that the size-sieving effect rather than adsorption during filtration dominates the rejection of the membranes. This is because the adsorption of particles on the BCP layer would certainly block pores, resulting in a corresponding great decline in permeability.

It should be noted that the membranes produced in this work exhibit much tighter selectivities but comparable water permeabilities compared to conventional membranes of electrospun nanofibers which typically provide separation in the MF category. For example, the cellulose nanowhisker-based nanofibrous membrane exhibited a good water permeability of 5900 L m^{-2} h^{-1} bar^{-1}; however, it failed to completely repel particles with diameter as large as 200 nm because of their poor selectivity.[43] Furthermore, the UF membranes produced by selective swelling of electrospun BCP nanofibers are superior in terms of both permeability and rejection to UF membranes prepared by grafting hydrogel onto nanofibrous substrates. For instance, it has been reported that grafting of poly(2-hydroxyethyl methacrylate) onto the surface of regenerated cellulose nanofibrous substrates could lead to UF membranes. However, thus-produce UF membranes displayed a permeability of <50 L m^{-2} h^{-1} bar^{-1} and an ~30% rejection to 40 nm particles.[16] For conventional membranes of electrospun nanofibers, the fiber layers usually have a thickness of a few tens or hundreds of micrometers, and the polymers are frequently hydrophobic ones. In contrast, the BCP layers for the membranes in this work are just a few micrometers in thickness, and the surfaces are highly hydrophilic as a result of the surface enrichment of the P2VP blocks. The thin thickness and the hydrophilic surface of the BCP selective layers on top of macroporous substrates greatly facilitate water permeation. More importantly, the pores in conventional membranes of electrospun fibers are usually larger than several hundreds of nanometers; therefore, the membranes only reject big particles with micrometer sizes. The membranes prepared in this study possess pore sizes lower than 100 nm, and consequently they deliver UF selectivities. Moreover, even compared to commercial PVDF UF membranes which possess water permeabilities ranging from ~157 to 176 L m^{-2} h^{-1} bar^{-1} (molecular weight cutoff: 500 000 Da),[44] our membranes remarkably show ~10−35 times higher water permeabilities while the rejection properties are similar. The composite membrane was subjected to ultrasonication oscillation in water at the power of 150 W for 10 min to test its robustness. We did not observe noticeable detachment of the BCP layer from the PVDF substrate, and there was no change in the morphology of the BCP layer under SEM before and after ultrasonication (Figure S5), indicating the strong adhesion of the BCP layer onto the substrate and the robustness of the composite membrane.

pH-Responsiveness of the Membranes from Electrospun BCP Nanofibers. Because P2VP blocks are enriched on the pore walls of the nanoporous BCP selective layers and P2VP is a weak polybase with a pK_a of ~4.5,[45] the effective pore sizes are dependent on the environmental pHs as a consequence of the protonation and deprotonation of pyridyl groups, leading to correspondingly tunable water permeabilities. The water permeability of the membrane produced from an electrospinning duration of 0.5 h was measured under pHs ranging from ~2 to 8. As can be seen in Figure 10a, the water permeability is as low as ~513 L m^{-2} h^{-1} bar^{-1} under a low pH

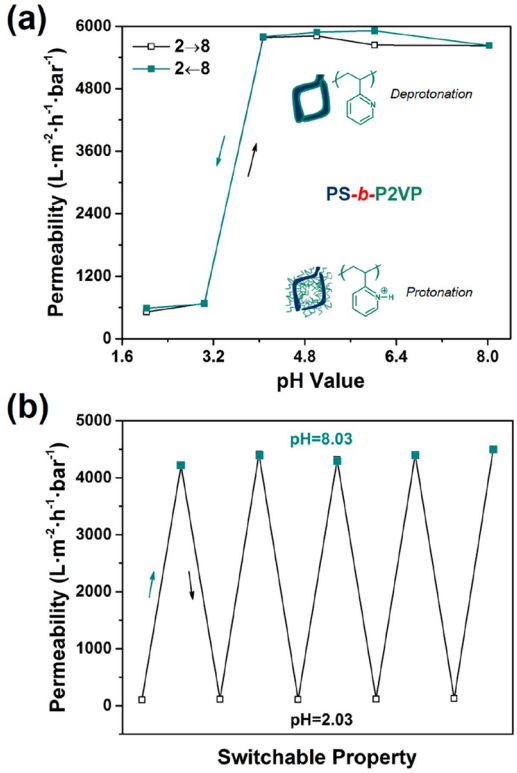

Figure 10. (a) Water permeability of the membrane produced from an electrospinning duration of 0.5 h as a function of varied pHs. Insets are illustrations presenting the protonation and deprotonation of the P2VP chains. (b) Changes of water permeabilities of the membrane produced from an electrospinning duration of 1 h with pH values switched between 2.03 and 8.03 for five cycles.

of 2.03. With pH increased to 3.04, the permeability is slightly increased to ~678 L m^{-2} h^{-1} bar^{-1}. Under pHs lower than the pK_a of P2VP, the pyridyl groups on P2VP chains enriched on the surface of the BCP struts defining the membrane pores become protonated. The electrostatic repulsion between protonated pyridyl groups causes the P2VP chains to take an extended conformation (the illustration in Figure 10a),[46] leading to shrunk effective pore sizes. Consequently, a reduction in the water permeability occurs. However, in other studies using BCPs containing pyridyl groups, the resultant membranes showed ignorable water permeability close to zero under low pH conditions.[47] Considering the large initial pore size and thin functional BCP top layer, a relatively large permeability exhibiting in the present study can be easily understood. In comparison, the pyridyl groups would be deprotonated under pHs higher than the pK_a of P2VP. As a consequence, the stretched P2VP chains would collapse and return to the initial state (insets in Figure 10a), resulting in the recovery of water permeability. As expected, the permeability of the membrane recovers to the original value of ~5815 L m^{-2} h^{-1} bar^{-1} and does not exhibit a noticeable change with increased pH value up to 8.03. That is there is a remarkable change in water permeability of more than 10 times when the pH is increased from 2.03 to 8.03. Additionally, such a pH-dependent water permeability is reversible as confirmed by the permeability tests performed with pHs decreased from 8.03 to 2.03. It should be noted that the permeability of our membranes can be adjusted from ~513 to ~5815 L m^{-2} h^{-1} bar^{-1} by changing pHs. To the best of our knowledge, this is

DOI: 10.1021/acs.macromol.8b00220
Macromolecules 2018, 51, 2283−2292

the widest range in the adjustment of the pH-dependent water permeability that has been achieved so far. Subsequently, we switched the pHs between 2.03 and 8.03 for five cycles and tested the water permeabilities at each cycle. As shown in Figure 10b, the membrane exhibits almost the same permeability at the switched pHs of 2.03 and 8.03 at each cycle, demonstrating the long-standing and stable pH responsiveness of our membranes.

CONCLUSION

Nanofibers of amphiphilic block copolymers of PS-*b*-P2VP were produced by electrospinning. Upon being soaked in hot ethanol, the fibers experience a morphology transition from solid nanofibers to perforated fibers with increased porosities and finally to isolated spherical micelles with progressively increasing degrees of swelling. The electrospun BCP nanofibers are used as building blocks to prepare UF membranes with pore sizes down to a few tens of nanometers. Heating the stacked nanofibers on top of macroporous substrates at the temperature slightly higher than T_g's of both blocks transforms the porous fiber layers to continuous films with a dense morphology. By subsequent ethanol swelling, we obtain homogeneous nanoporous BCP layers with uniform thicknesses tightly adhering to the macroporous substrates. The thicknesses of the nanoporous layers can be linearly tuned from ∼2 to ∼10 μm simply by extending the durations of electrospinning from 0.5 to 2 h. The pores are formed as a result of the selective swelling of the P2VP microdomains confined in the PS matrix. Inherent to the mechanism of selective-swelling-induced pore generation, the polar P2VP blocks are enriched on the surfaces, which endows a strong hydrophilicity to the membranes. Owing to the thin thickness of the BCP selective layers and the strong surface hydrophilicity, the composite membranes with BCP nanoporous selective layers on top of the macroporous PVDF substrate deliver excellent UF performances. The permeability and rejection properties can be readily tuned by altering the electrospinning durations, and an electrospinning duration of 0.5 h produces a water permeability high than 6100 L m^{-2} h^{-1} bar^{-1} and a rejection rate of 78% to 22 nm silica nanospheres. Such a water permeability is 1−2 orders of magnitude higher than commercial UF membranes with similar rejections. Moreover, because of the enrichment of P2VP blocks on the surface and pore walls, the membranes exhibit a sharp pH-dependence in water permeabilities which can be remarkably shifted between ∼500 and ∼6000 L m^{-2} h^{-1} bar^{-1} for multiple cycles with pH values changed between ∼2 and 8. The thus-produced membrane offers significant opportunities for high-flux membrane separation with a pH-responsive function. Importantly, considering the facts that almost every polymer can be electrospun to produce nanofibers and many amphiphilic block copolymers have been demonstrated to be cavitated by the selective swelling process, we believe the method reported here is versatile in preparing UF membranes of different block copolymers. Especially, we expect it can be expanded to prepare high-flux membranes for practical applications from more suitable block copolymers, for instance, polysulfone-based ones which are currently available in large scale at affordable costs.[48]

MATERIALS AND METHODS

Materials. The block copolymer of PS-*b*-P2VP [M_n(PS) = 53 000 g mol^{-1}, M_n(P2VP) = 21 000 g mol^{-1}, polydispersity index (PDI) = 1.17] was purchased from Tubang Polymer Materials Co., Ltd. Sodium hydroxide (NaOH, 96 wt %), LiCl (97 wt %), ethanol (99.7 wt %), *N*,*N*-dimethylformamide (DMF, 99.5 wt %), hydrochloric acid (HCl, 37 wt %), and chloroform (99 wt %) were obtained from local suppliers. Monodispersed silica (SiO_2) nanospheres with the size of 22 nm, dispersed in water, were purchased from Sigma-Aldrich and diluted before filtration application. The silicon wafers, which served as the substrates to characterize the morphology of individual fibers, were obtained from Zhejiang Guifeng Electronics Ltd. A negatively charged dye, AO7, was purchased from Aladdin with a purity >85%. PVDF membranes with a nominal pore size of ∼0.22 μm were sourced form Tianjin Jinteng and were used as the substrates to prepare composite membranes. Deionized water (conductivity: 8−20 μs/cm, Wahaha) was used in all the experiments. All the chemicals were used without further purification.

Electrospinning of BCP Nanofibers. PS-*b*-P2VP was first dissolved in a 3:1 mixture by mass ratio of chloroform and DMF to a concentration of 20 wt %. Inorganic salt of LiCl was then added into the BCP solution to the concentration of 0.03 wt %, followed by a mild stirring for at least 12 h. The electrospinning was operated in the closed chamber of an electrospinning device (FM-1206, Beijing Future Material Sci-tech Co. Ltd.) at the temperature of 25 ± 5 °C and the humidity of 30 ± 5%. The BCP solution was injected at a feeding rate of 0.01 mm s^{-1} under the voltage of 20 kV with two injectors controlled independently by two syringe pumps. To have better observations on the individual fibers, the fibers were spun for about 1 min and collected on the cleaned silicon wafers (1.5 cm × 1.5 cm). To prepare the fibrous membranes, the fibers were collected by a roller with a rotational speed of ∼800 rpm. A stepping motor was used to control the translational movement of the spinneret to ensure an uniform thickness of the resulting fiber layers. In addition, the electrospinning duration was varied from 0.5 to 2 h in order to achieve a controllable thickness of the fiber mat. The silicon wafer or the roller was placed at a distance of 15 cm below the tip of the spinneret.

Swelling of BCP Electrospun Nanofibers in Ethanol. The BCP nanofibers collected on silicon wafers were immersed in ethanol to perform selective swelling at the temperature of 70 or 75 °C for different durations. The samples were then withdrawn from ethanol and dried in air at room temperature for subsequent characterizations.

Preparation of UF Membranes from BCP Electrospun Nanofibers. The schematic diagram of the preparation process is illustrated in Figure 1. After spinning, the BCP fiber layers can be easily peeled off from the roller. The fiber layers removed from the roller were placed on macroporous PVDF substrates and then thermally treated at 110 °C for 1 h to enhance both mechanical stability among fibers and adhesion between the fibers and the substrates. Thus-produced composite structures with various thicknesses of fiber layers were immersed in ethanol 70 °C for 6 h to generate pores in the fiber layers, thus producing composite membranes with nanoporous BCP separation layers on top of macroporous PVDF membranes.

Characterizations. The surface and cross-sectional morphology of the electrospun BCP fibers and the composite membranes before and after swelling were observed by SEM (S-4800, Hitachi) operated at the accelerating voltage of 5 kV. The samples for cross-sectional examinations were obtained by fracturing in liquid nitrogen. Prior to SEM characterization, the samples were sputter-coated with a thin layer of platinum to enhance their conductivity. The diameter of the electrospun BCP fibers was measured by using image analysis software (Nano Measurer) according to the SEM images. A contact angle goniometer (DropMeter A100, Maist) was used to characterize the dynamic WCAs of the BCP layers on the PVDF substrates. XPS was performed on an ESCALAB 250 XPS system (Thermo Scientific) with a monochromatic Al Kα X-ray source (1486.6 eV photons) to probe the surface chemical compositions of the BCP layers before and after swelling.

Filtration Tests. The water permeabilities and retention performances of resultant membranes were tested using a stirred filtration setup (Amicon8003, Millipore). Precompaction of the composite membranes at 0.4 bar for 10 min before testing at the same trans-

DOI: 10.1021/acs.macromol.8b00220
Macromolecules 2018, 51, 2283−2292

membrane pressure (TMP) was performed to ensure a stable permeability. Deionized water was used to measure the pure water permeability, and silica nanospheres with the diameter of 22 nm were served as the media to estimate the retention performances of the membranes. Before retention tests, the membranes were filtrated with 10 mL of anionic AO7 solution (5 mg L^{-1}) and then washed thoroughly with deionized water to neutralize the originally positively charged membranes surface to eliminate any adsorption effects. The concentrations of silica nanospheres in feeds, permeations, and retentions, were analyzed via inductively coupled plasma optical emission spectrometry (Optima 7000DV, PerkinElmer). The rejection rates were calculated by the following equation:

$$\%R = 100 \times (1 - C_p/C_f) \quad (2)$$

where C_p and C_f are silica concentrations in the permeation and the feed, respectively. The pH-dependent permeabilities of the membranes were also measured at a decreased TMP of 0.2 bar to minimize the compaction effect. Water solutions with varied pH values were obtained by the addition of HCl or NaOH. A thorough prewashing of the membrane and filtration cell was conducted with the solution used next time before switching to another pH condition.

■ ASSOCIATED CONTENT

Supporting Information

The Supporting Information is available free of charge on the ACS Publications website at DOI: 10.1021/acs.macromol.8b00220.

Additional experimental images (Figures S1–S5) and table (Table S1) (PDF)

■ AUTHOR INFORMATION

Corresponding Author

*E-mail: yongwang@njtech.edu.cn (Y.W.).

ORCID

Yong Wang: 0000-0002-8653-514X

Author Contributions

X.S. and Z.X. contributed equally to this work.

Notes

The authors declare no competing financial interest.

■ ACKNOWLEDGMENTS

Financial support from the National Basic Research Program of China (2015CB655301), Natural Science Foundation of China (21776126), the Jiangsu Natural Science Foundation (BK20150063), and the Program of Excellent Innovation Teams of Jiangsu Higher Education Institutions is gratefully acknowledged.

■ REFERENCES

(1) Sill, T. J.; von Recum, H. A. Electrospinning: Applications in Drug Delivery and Tissue Engineering. *Biomaterials* **2008**, *29*, 1989–2006.

(2) Mouthuy, P. A.; Ye, H.; Triffitt, J.; Oommen, G.; Cui, Z. Physico-Chemical Characterization of Functional Electrospun Scaffolds for Bone and Cartilage Tissue Engineering. *Proc. Inst. Mech. Eng., Part H* **2010**, *224*, 1401–1414.

(3) Liu, C.; Hsu, P. C.; Lee, H. W.; Ye, M.; Zheng, G.; Liu, N.; Li, W.; Cui, Y. Transparent Air Filter for High-Efficiency PM2.5 Capture. *Nat. Commun.* **2015**, *6*, 6205.

(4) Wang, C.; Wu, S.; Jian, M.; Xie, J.; Xu, L.; Yang, X.; Zheng, Q.; Zhang, Y. Silk Nanofibers as High Efficient and Lightweight Air Filter. *Nano Res.* **2016**, *9*, 2590–2597.

(5) Zhang, R.; Liu, C.; Hsu, P. C.; Zhang, C.; Liu, N.; Zhang, J.; Lee, H. R.; Lu, Y.; Qiu, Y.; Chu, S.; Cui, Y. Nanofiber Air Filters with High-Temperature Stability for Efficient PM2.5 Removal from the Pollution Sources. *Nano Lett.* **2016**, *16*, 3642–3649.

(6) Mouthuy, P. A.; El-Sherbini, Y.; Cui, Z.; Ye, H. Layering PLGA-based Electrospun Membranes and Cell Sheets for Engineering Cartilage-Bone Transition. *J. Tissue Eng. Regener. Med.* **2016**, *10*, E263–E274.

(7) Yoon, K.; Hsiao, B. S.; Chu, B. Functional Nanofibers for Environmental Applications. *J. Mater. Chem.* **2008**, *18*, 5326–5334.

(8) Tian, M.; Wang, Y.-N.; Wang, R. Synthesis and Characterization of Novel High-Performance Thin Film Nanocomposite (TFN) FO Membranes with Nanofibrous Substrate Reinforced by Functionalized Carbon Nanotubes. *Desalination* **2015**, *370*, 79–86.

(9) Ma, H.; Burger, C.; Hsiao, B. S.; Chu, B. Ultra-Fine Cellulose Nanofibers: New Nano-Scale Materials for Water Purification. *J. Mater. Chem.* **2011**, *21*, 7507–7510.

(10) Qiu, X.; Yu, H.; Karunakaran, M.; Pradeep, N.; Nunes, S. P.; Peinemann, K.-V. Selective Separation of Similarly Sized Proteins with Tunable Nanoporous Block Copolymer Membranes. *ACS Nano* **2013**, *7*, 768–776.

(11) Jackson, E. A.; Hillmyer, M. A. Nanoporous Membranes Derived from Block Copolymers: from Drug Delivery to Water Filtration. *ACS Nano* **2010**, *4*, 3548–3553.

(12) Wang, X.; Fang, D.; Yoon, K.; Hsiao, B. S.; Chu, B. High Performance Ultrafiltration Composite Membranes Based on Poly(vinyl alcohol) Hydrogel Coating on Crosslinked Nanofibrous Poly(vinyl alcohol) Scaffold. *J. Membr. Sci.* **2006**, *278*, 261–268.

(13) Yoon, K.; Kim, K.; Wang, X.; Fang, D.; Hsiao, B. S.; Chu, B. High Flux Ultrafiltration Membranes Based on Electrospun Nanofibrous PAN Scaffolds and Chitosan Coating. *Polymer* **2006**, *47*, 2434–2441.

(14) Wang, X.; Chen, X.; Yoon, K.; Fang, D.; Hsiao, B. S.; Chu, B. High Flux Filtration Medium Based on Nanofibrous Substrate with Hydrophilic Nanocomposite Coating. *Environ. Sci. Technol.* **2005**, *39*, 7684–7691.

(15) Yang, Y.; Li, X.; Shen, L.; Wang, X.; Hsiao, B. S. Ionic Cross-Linked Poly(acrylonitrile-co-acrylic acid)/Polyacrylonitrile Thin Film Nanofibrous Composite Membrane with High Ultrafiltration Performance. *Ind. Eng. Chem. Res.* **2017**, *56*, 3077–3090.

(16) Wang, Z.; Crandall, C.; Prautzsch, V. L.; Sahadevan, R.; Menkhaus, T. J.; Fong, H. Electrospun Regenerated Cellulose Nanofiber Membranes Surface-Grafted with Water-Insoluble Poly(HEMA) or Water-Soluble Poly(AAS) Chains via the ATRP Method for Ultrafiltration of Water. *ACS Appl. Mater. Interfaces* **2017**, *9*, 4272–4278.

(17) Chen, W.; Wei, M.; Wang, Y. Advanced Ultrafiltration Membranes by Leveraging Microphase Separation in Macrophase Separation of Amphiphilic Polysulfone Block Copolymers. *J. Membr. Sci.* **2017**, *525*, 342–348.

(18) McCann, J. T.; Marquez, M.; Xia, Y. Highly Porous Fibers by Electrospinning into a Cryogenic Liquid. *J. Am. Chem. Soc.* **2006**, *128*, 1436–1437.

(19) Zhao, H.; Gu, W.; Thielke, M. W.; Sterner, E.; Tsai, T.; Russell, T. P.; Coughlin, E. B.; Theato, P. Functionalized Nanoporous Thin Films and Fibers from Photocleavable Block Copolymers Featuring Activated Esters. *Macromolecules* **2013**, *46*, 5195–5201.

(20) Wang, Y. Nondestructive Creation of Ordered Nanopores by Selective Swelling of Block Copolymers: toward Homoporous Membranes. *Acc. Chem. Res.* **2016**, *49*, 1401–1408.

(21) Wang, Y.; Tong, L.; Steinhart, M. Swelling-Induced Morphology Reconstruction in Block Copolymer Nanorods: Kinetics and Impact of Surface Tension during Solvent Evaporation. *ACS Nano* **2011**, *5*, 1928–1938.

(22) Wang, Y.; He, C.; Xing, W.; Li, F.; Tong, L.; Chen, Z.; Liao, X.; Steinhart, M. Nanoporous Metal Membranes with Bicontinuous Morphology from Recyclable Block-Copolymer Templates. *Adv. Mater.* **2010**, *22*, 2068–2072.

(23) Guo, L.; Wang, X.; Wang, Y. Facile Synthesis of Bimodal Nanoporous Carbons by Templating Selective Swelling-Induced Mesoporous Block Copolymers. *Chem. Eng. J.* **2017**, *313*, 1295–1301.

DOI: 10.1021/acs.macromol.8b00220
Macromolecules 2018, 51, 2283–2292

(24) Yan, N.; Wang, Y. Selective Swelling Induced Pore Generation of Amphiphilic Block Copolymers: The Role of Swelling Agents. *J. Polym. Sci., Part B: Polym. Phys.* **2016**, *54*, 926−933.
(25) Wang, Y.; Qin, Y.; Berger, A.; Yau, E.; He, C.; Zhang, L.; Gösele, U.; Knez, M.; Steinhart, M. Nanoscopic Morphologies in Block Copolymer Nanorods as Templates for Atomic-Layer Deposition of Semiconductors. *Adv. Mater.* **2009**, *21*, 2763−2766.
(26) Liao, Y.; Wang, R.; Tian, M.; Qiu, C.; Fane, A. G. Fabrication of Polyvinylidene fluoride (PVDF) Nanofiber Membranes by Electrospinning for Direct Contact Membrane Distillation. *J. Membr. Sci.* **2013**, *425−426*, 30−39.
(27) Wei, M.; Sun, W.; Shi, X.; Wang, Z.; Wang, Y. Homoporous Membranes with Tailored Pores by Soaking Block Copolymer/Homopolymer Blends in Selective Solvents: Dissolution versus Swelling. *Macromolecules* **2016**, *49*, 215−223.
(28) Wang, Y.; Li, F. An Emerging Pore-Making Strategy: Confined Swelling-Induced Pore Generation in Block Copolymer Materials. *Adv. Mater.* **2011**, *23*, 2134−2148.
(29) Bates, F. S.; Fredrickson, G. H. Block copolymers-Designer soft materials. *Phys. Today* **1999**, *52*, 32−38.
(30) Yang, Z.; Wang, Z.; Yao, X.; Wang, Y. Water-Dispersible, Uniform Nanospheres by Heating-Enabled Micellization of Amphiphilic Block Copolymers in Polar Solvents. *Langmuir* **2012**, *28*, 3011−3017.
(31) Kimmins, S. D.; Cameron, N. R. Functional Porous Polymers by Emulsion Templating: Recent Advances. *Adv. Funct. Mater.* **2011**, *21*, 211−225.
(32) Pulko, I.; Wall, J.; Krajnc, P.; Cameron, N. R. Ultra-High Surface Area Functional Porous Polymers by Emulsion Templating and Hypercrosslinking: Efficient Nucleophilic Catalyst Supports. *Chem. - Eur. J.* **2010**, *16*, 2350−2354.
(33) Phillip, W. A.; Rzayev, J.; Hillmyer, M. A.; Cussler, E. L. Gas and Water Liquid Transport Through Nanoporous Block Copolymer Membranes. *J. Membr. Sci.* **2006**, *286*, 144−152.
(34) Chen, Q.; Luo, M.; Hammershoj, P.; Zhou, D.; Han, Y.; Laursen, B. W.; Yan, C.-G.; Han, B.-H. Microporous Polycarbazole with High Specific Surface Area for Gas Storage and Separation. *J. Am. Chem. Soc.* **2012**, *134*, 6084−6087.
(35) Abidian, M. R.; Kim, D. H.; Martin, D. C. Conducting-Polymer Nanotubes for Controlled Drug Release. *Adv. Mater.* **2006**, *18*, 405−409.
(36) Lu, H.; Lee, D. H.; Russell, T. P. Temperature Tunable Micellization of Polystyrene-*block*-Poly(2-vinylpyridine) at Si-Ionic Liquid Interface. *Langmuir* **2010**, *26*, 17126−17132.
(37) Homaeigohar, S.; Koll, J.; Lilleodden, E. T.; Elbahri, M. The Solvent Induced Interfiber Adhesion and Its Influence on the Mechanical and Filtration Properties of Polyethersulfone Electrospun Nanofibrous Microfiltration Membranes. *Sep. Purif. Technol.* **2012**, *98*, 456−463.
(38) Wang, Z.; Yao, X.; Wang, Y. Swelling-Induced Mesoporous Block Copolymer Membranes with Intrinsically Active Surfaces for Size-Selective Separation. *J. Mater. Chem.* **2012**, *22*, 20542−20548.
(39) Kim, J.; Lew, B.; Kim, W. S. Facile Fabrication of Super-Hydrophobic Nano-Needle Arrays via Breath Figures Method. *Nanoscale Res. Lett.* **2011**, *6*, 616−623.
(40) Sun, W.; Wang, Z.; Yao, X.; Guo, L.; Chen, X.; Wang, Y. Surface-Active Isoporous Membranes Nondestructively Derived from Perpendicularly Aligned Block Copolymers for Size-Selective Separation. *J. Membr. Sci.* **2014**, *466*, 229−237.
(41) Cassie, A. B. D.; Baxter, S. Wettability of Porous Surfaces. *Trans. Faraday Soc.* **1944**, *40*, 546−551.
(42) Yao, X.; Guo, L.; Chen, X.; Huang, J.; Steinhart, M.; Wang, Y. Filtration-Based Synthesis of Micelle-Derived Composite Membranes for High-Flux Ultrafiltration. *ACS Appl. Mater. Interfaces* **2015**, *7*, 6974−6981.
(43) Ma, H.; Burger, C.; Hsiao, B. S.; Chu, B. Nanofibrous Microfiltration Membrane Based on Cellulose Nanowhiskers. *Biomacromolecules* **2012**, *13*, 180−186.
(44) SY A6 Ultrafiltration (UF) Membrane, Sepa CF Size; http://www.sterlitech.com/flat-sheet-membranes-specifications.html#UF, accessed Oct 2017.
(45) Li, J. J.; Zhou, Y. N.; Luo, Z. H. Smart Fiber Membrane for pH-Induced Oil/Water Separation. *ACS Appl. Mater. Interfaces* **2015**, *7*, 19643−19650.
(46) Yi, Z.; Zhang, P.-B.; Liu, C.-J.; Zhu, L.-P. Symmetrical Permeable Membranes Consisting of Overlapped Block Copolymer Cylindrical Micelles for Nanoparticle Size Fractionation. *Macromolecules* **2016**, *49*, 3343−3351.
(47) Hahn, J.; Clodt, J. I.; Abetz, C.; Filiz, V.; Abetz, V. Thin Isoporous Block Copolymer Membranes: It Is All about the Process. *ACS Appl. Mater. Interfaces* **2015**, *7*, 21130−21137.
(48) Wang, Z. G.; Liu, R.; Yang, H.; Wang, Y. Nanoporous Polysulfones with In Situ PEGylated Surfaces by A Simple Swelling Strategy Using Paired Solvents. *Chem. Commun.* **2017**, *53*, 9105−9108.

DOI: 10.1021/acs.macromol.8b00220
Macromolecules 2018, 51, 2283−2292